

RESEARCH ARTICLE

10.1002/2013JA019619

Key Points:

- Spatial coherence scale of ground scintillation pattern
- Intermediate scale irregularity spectrum in equatorial plasma bubble
- Season and solar flux dependence of irregularity spectrum

Correspondence to:

A. Bhattacharyya,
abh@iigs.igm.res.in

Citation:

Bhattacharyya, A., B. Kakad, S. Sripathi, K. Jeeva, and K. U. Nair (2014), Development of intermediate scale structure near the peak of the *F* region within an equatorial plasma bubble, *J. Geophys. Res. Space Physics*, 119, 3066–3076, doi:10.1002/2013JA019619.

Received 13 NOV 2013

Accepted 26 FEB 2014

Accepted article online 3 MAR 2014

Published online 2 APR 2014

Development of intermediate scale structure near the peak of the *F* region within an equatorial plasma bubble

A. Bhattacharyya¹, B. Kakad¹, S. Sripathi¹, K. Jeeva¹, and K. U. Nair¹

¹Indian Institute of Geomagnetism, Navi Mumbai, Maharashtra, India

Abstract Scintillation observations are used to study the evolution of intermediate scale (~100 m–few kilometers) irregularities through growth of the Rayleigh-Taylor (R-T) instability on the bottom side of the post-sunset equatorial *F* region during magnetically quiet periods. Amplitude scintillations on a VHF signal from a geostationary satellite, recorded by spaced receivers at an equatorial station, are used to compute as a function of local time: (1) the coherence scale length for spatial variations of intensity in the ground scintillation pattern, which is linked with the spectrum of the intermediate scale irregularities near the peak of the equatorial *F* region that contribute the most to the observed scintillations; and (2) the “random velocity”, which accounts for the de-correlation of the spaced receiver signals. The relationship between the coherence scale length and the random velocity for saturated scintillations at different local times suggests that (1) the random velocity is linked with fluctuations in the drift velocity of the irregularities caused by the perturbation electric fields associated with the R-T instability rather than structural changes in the intermediate scale irregularities, (2) the spectrum of intermediate scale irregularities in the equatorial *F* peak region tends to be shallowest after the decay of the perturbation electric fields associated with the R-T instability, and (3) evolution of intermediate-scale irregularity spectrum in the equatorial plasma bubble near the equatorial *F* region peak depends on season and solar flux. These have implications for observation of low-latitude L-band scintillations.

1. Introduction

In low-latitude regions, strength and latitudinal extent of post-sunset ionospheric scintillations on VHF and higher frequency trans-ionospheric radio signals depend on the spectrum of intermediate-scale (~100 m–few kilometers) ionospheric irregularities at different heights within an equatorial plasma bubble (EPB), the maximum height of the irregularities over the dip equator, and the ambient plasma density. The scale sizes referred to here are in the plane transverse to the signal path. Any effort to forecast scintillations on such signals recorded in low-latitude regions requires a knowledge of the dynamics of the irregularities and of the evolution of intermediate-scale irregularities within an EPB as it rises and emerges into the topside ionosphere [Costa *et al.*, 2011]. In numerical simulations of the development of EPBs due to growth of the Rayleigh-Taylor (R-T) instability in the post-sunset equatorial ionosphere, spatial resolution is not adequate to yield the irregularity spectrum in the intermediate-scale range, and an extrapolation of the spectrum of fluctuations in the vertical total electron content (TEC) down to the intermediate-scale sizes is required to forecast scintillations [Retterer, 2010a, 2010b]. Results obtained from such a 3-D simulation of the EPBs or plasma plumes, as shown in Figure 2 of Retterer [2010b], indicate that the spectral density of fluctuations in vertical TEC, down to a magnetic east-west wavelength of 10 km, evolves differently at different geomagnetic latitudes. According to these results, in the early stages of EPB development before approximately 22 h local time (LT), when the low-density region rises rapidly to form a plume, which bifurcates to produce smaller scale structures, the spectrum is steepest at the geomagnetic equator and shallowest at a geomagnetic latitude of 16°. The fluctuations in vertical TEC in any region have maximum contribution from irregularities near the *F* layer peak. Hence, numerical simulations [Retterer, 2010a, 2010b] indicate that within the EPBs, the *F* layer peak in the equatorial ionization anomaly (EIA) crest region is more structured than the equatorial *F* layer peak before 22 LT. However, after 22 LT, shorter scale irregularities appear to develop in and around the equatorial *F* layer peak so that the spectrum of vertical TEC fluctuations at the geomagnetic equator becomes shallower, even while the spectra at off-equatorial locations become steeper. The latter may also be attributed to the fact that by this time the perturbation electric field associated with the R-T instability has decayed and the irregularities embedded in the EPBs now descend with the ambient *F* layer and the topside irregularities over the geomagnetic equator are no longer mapped

to higher geomagnetic latitudes. This picture of the evolution of structure of scale sizes greater than 10 km in EPBs indicates that at the geomagnetic equator, an EPB in its initial stage of development before 22 LT may have more structure near its top than near the F layer peak. In case such a scenario holds also for intermediate-scale structures in EPBs, it would have ramifications for the occurrence of scintillations on VHF and higher frequency radio signals recorded in low-latitude regions [Valladares *et al.*, 2004].

Observations of significant L-band scintillations near the crest of the EIA region, when L-band scintillations are absent in the dip equatorial region, although strong scintillations on a VHF signal are recorded there, have been attributed to the higher ambient plasma density near the EIA crest [Mullen *et al.*, 1985; Groves *et al.*, 1997; Bhattacharyya *et al.*, 2003; Sripathi *et al.*, 2008]. The S_4 index, which is the standard deviation of normalized intensity fluctuations computed from amplitude scintillation data, saturates with increasing strength of the irregularities. Hence, when scintillations are saturated on a VHF signal, the S_4 index computed for this signal does not track the strength of the irregularities. Basu *et al.* [1983] found that the S_4 index for L-band scintillations recorded at Ascension Island, near the crest of the EIA, was inversely correlated with the coherence time of saturated VHF scintillations recorded at the same location. Earlier Rino and Owen [1980] had studied the time structure of transionospheric radio wave scintillation and obtained an approximate analytic expression for the coherence time (50% de-correlation time) of saturated intensity scintillations, which was dependent on the spectral index of the power law irregularity spectrum considered by them. Comparing this with observations, the authors concluded that data from Ancon (geomagnetic latitude 0.6°S) yield a slightly steeper irregularity spectrum than the Kwajalein (geomagnetic latitude 3.3°N) data. Franke and Liu [1985] obtained an approximate analytic expression for the spatial coherence scale length, d_i , of intensity variations in the reception plane under saturated scintillation conditions, for a two-component power law irregularity spectrum with one-dimensional power-spectral indices of 1 for scale lengths longer than, and 3 for scale lengths shorter than, the break scale length. They found that d_i was inversely proportional to the irregularity strength as measured by the standard deviation of electron density fluctuations, but the proportionality constant was dependent on the break scale. In both these papers evolution of the irregularity spectrum was not studied.

In this paper, various parameters computed from amplitude scintillation data on a VHF signal are used to specifically study the evolution of intermediate-scale irregularities in the equatorial and low-latitude ionosphere under different ambient conditions. Information derived from the spectrum of weak scintillations ($S_4 \leq 0.5$) from an equatorial and an off-equatorial location is presented in the next section. As the S_4 index on a VHF signal may often exceed 0.5 during the course of a scintillation event, additional insight into the evolution of the irregularity structure during the course of such an event is provided by the patterns of variation of the coherence scale length d_i computed from spaced receiver amplitude scintillation data [Bhattacharyya *et al.*, 2003]. The relationship between d_i and another parameter, the so-called random velocity V_C [Vacchione *et al.*, 1987; Spatz *et al.*, 1988; Bhattacharyya *et al.*, 1989] obtained from the same scintillation data at an equatorial station, during various stages of evolution of the irregularities on magnetically quiet days under different seasonal and solar flux conditions is also explored, since these two parameters are related to different characteristics of the irregularities. Results obtained are discussed in the context of in situ observations [Shume and Hysell, 2004; Rodrigues *et al.*, 2009; Xiong *et al.*, 2012].

2. Spectrum of Weak Scintillations

The parameters considered in this paper have been calculated using amplitude scintillation data for a 251 MHz signal transmitted from the geostationary satellite, UFO2, located at 71.2°E and recorded using two receivers spaced 540 m apart along a magnetic east-west baseline at the equatorial station Tirunelveli (8.7°N , 77.8°E , geomagnetic latitude 0.2°S) during June 2001 to January 2006. This has been supplemented by amplitude scintillation data for a 251 MHz signal transmitted from the geostationary satellite, FLEETSAT, located at 73°E and recorded in the same manner at Tirunelveli during some equinoctial and summer months of the years 1995–2000. The data have been sampled at intervals of 0.1 s. The azimuth and zenith angles of the signal paths for UFO2 (FLEETSAT) were 216.9° (209°) and 12.8° (11.4°), respectively. Amplitude scintillations on the same frequency recorded at an off-equatorial station Mumbai (19.01°N , 72.85°E , geomagnetic latitude 10.4°N) by a single receiver with 10 Hz sampling frequency have also been used to compute the spectra of weak scintillations.

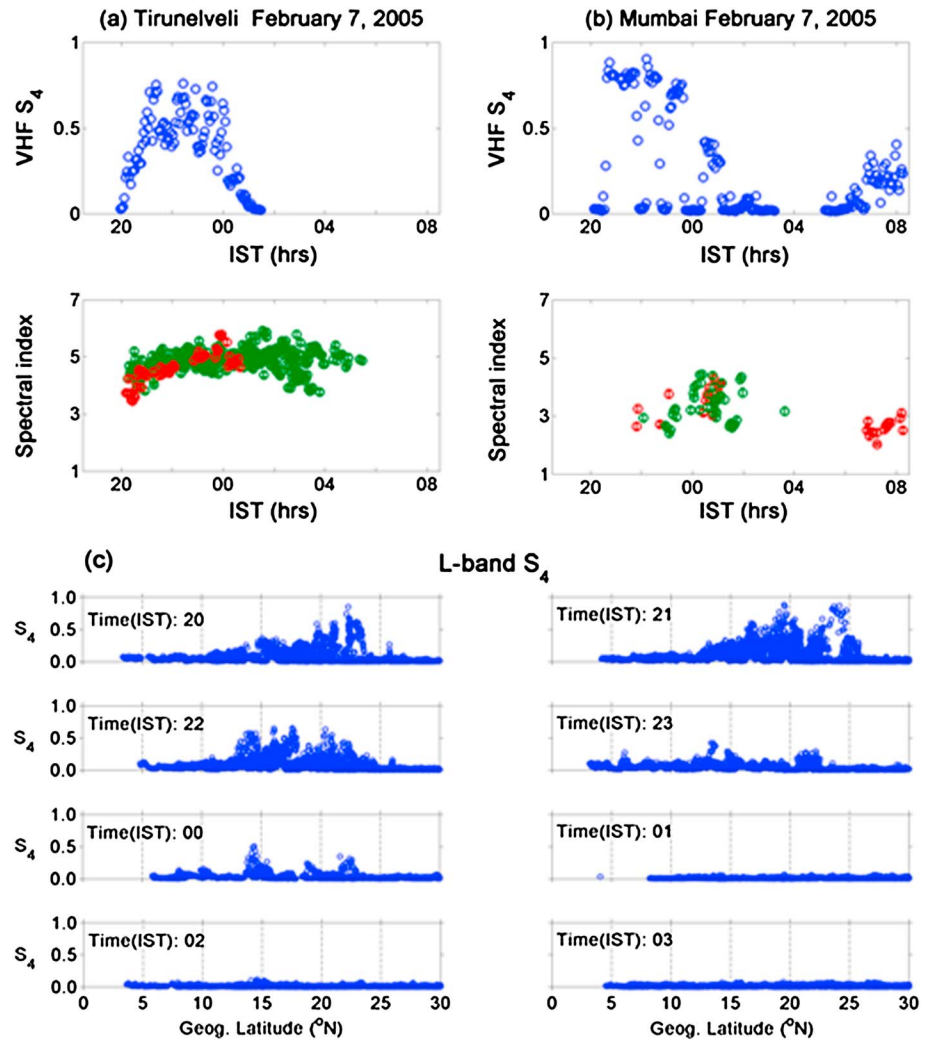


Figure 1. (a) Top panel: S_4 computed from amplitude scintillations on a VHF signal recorded at Tirunelveli (geomagnetic latitude 0.2° S) on a magnetically disturbed day, 7 February 2005; bottom panel: power spectral indices computed from weak amplitude scintillations ($S_4 \leq 0.5$). The red and green markers are for 7 February 2005, and quiet days in February 2005, respectively; Figure 1b same as Figure 1a for Mumbai (geomagnetic latitude 10.4° N); (c) latitudinal distribution of L-band scintillations in 75° E– 80° E longitude zone at different times (Indian standard time IST = UT + 5.5 h) during the night of 7 February 2005.

For an isotropic 3-D spatial power spectrum of the irregularities of the form $P_{\Delta N}(k) \propto k^{-(m+1)}$ valid between an inner and an outer scale, power spectrum of weak amplitude scintillations is of the form $P(f) \propto f^{-m}$ for frequencies f greater than the Fresnel frequency [Yeh and Liu, 1982]. The spatial scales and f are related by an effective drift speed V with which the ground scintillation pattern is perceived to move past a receiver, converting the spatial scales in the pattern into temporal scales in the data recorded by a receiver. The equatorial ionospheric irregularities are not isotropic being highly elongated along the geomagnetic field lines. The one-dimensional description of the irregularities provided by a satellite moving through them has been extended to two dimensions by fitting the satellite data to a more flexible 3-D power spectral density model, which included a break in slope [Costa et al., 2011]. These authors found the break in slope to occur at 80 m, which need not be considered for VHF scintillation spectra. For moderate and stronger scintillations, the relationship between the irregularity and scintillation spectra becomes more complex since multiple scattering and focusing of the radio signals come into play. In Figure 1, the top panels display plots of the S_4 indices computed for scintillations recorded at Tirunelveli and Mumbai on 7 February 2005, which was a magnetically disturbed day with $A_p = 30$. On this day, moderate scintillations were recorded at both the

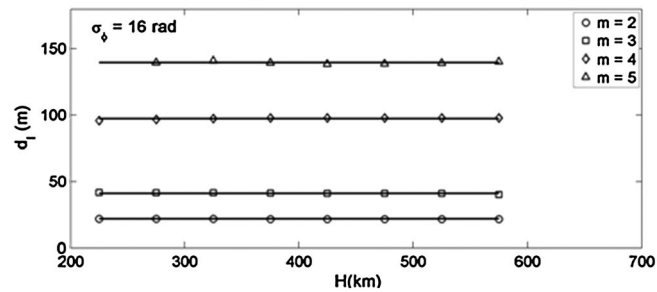


Figure 2. Variation of the coherence scale d_l in the saturated scintillation regime ($S_4 \geq 1$), with the average height H of the irregularity layer. The modeled irregularities have two-dimensional power law spectra with indices $m = 2, 3, 4$, and 5 . In all the cases, standard deviation of phase fluctuations imposed by the irregularity layer is 16 radians, and the thickness of the irregularity layer and outer scale for the power law spectrum are 50 km and 10 km, respectively.

locations. The bottom panels show the spectral indices computed for 3 min intervals of weak scintillations ($0.15 \leq S_4 \leq 0.5$) recorded at the two locations for this day superposed on similarly computed spectral indices for all the magnetically quiet days with scintillations in February 2005. Intervals with S_4 indices lower than 0.15 have a low signal-to-noise ratio and therefore have been excluded. The frequency range over which the spectral index is computed extends from the Fresnel frequency to around 1 Hz. The Fresnel frequency depends on the speed with which the ground scintillation pattern drifts past the receiver and hence may vary with time. Detailed information about the derivation of spectral indices may be found in *Kakad et al.* [2012] and several other references mentioned there. According to this figure, spectral indices obtained at Mumbai are lower than those obtained at the equatorial station for all the days considered. Magnetic disturbances on 7 February 2005 caused the equatorial F layer in this region to rise at around 20 LT yielding $h'F$ of about 400 km compared to an average $h'F \sim 300$ km for all the magnetically quiet days of February 2005, and after returning to the quiet time heights, the F region rose again around 06 LT with $h'F$ reaching 450 km [*Kakad et al.*, 2012]. The irregularities generated as a result of this height rise also have a shallower spectrum at the higher geomagnetic latitude but produce only weak scintillations on a VHF signal. Latitudinal distribution of L-band scintillations recorded at different times during the night of 7 February 2005, in the 75–80°E longitude zone using a network of GPS receivers in the Indian region, is shown in Figure 1c. This figure shows that while L-band scintillations were nearly absent over the dip equator in this region (geographic latitude $\approx 8^\circ\text{N}$) and up to a geographic latitude of 12°N , moderate to strong L-band scintillations are seen at higher latitudes up to 25°N (geomagnetic latitude $\approx 16^\circ\text{N}$) until about 22 LT. L-band scintillations decrease significantly after 22 LT. In order to understand this pattern of occurrence of L-band scintillations, it is necessary to explore the evolution of the irregularity spectra over the dip equator, where the EPB is initiated. At a time when L-band scintillations in the equatorial region are so weak that the L-band $S_4 < 0.15$ and the L-band scintillation spectrum is dominated by noise, substantially greater scintillations on a VHF signal may provide useful information. However, weak scintillation spectra need not represent the spectra of fully developed irregularities. In the next section, it is explored whether the variation of the coherence scale d_l provides any information about the evolution of the irregularity spectrum under strong scattering conditions.

3. Coherence Scale Length

Theoretical calculations of d_l have been carried out for a 251 MHz radio signal propagating perpendicular to a thick layer of essentially two-dimensional irregularities highly elongated along geomagnetic field lines, by solving the equation satisfied by the fourth moment of the complex amplitude of the signal [*Engavale and Bhattacharyya*, 2005] using the split-step method [*Bhattacharyya and Yeh*, 1988]. For weak scintillations, d_l is determined by the Fresnel scale length ($= \sqrt{2\lambda H}$, where λ is the signal wavelength and H is the average distance of the irregularity layer from the receiver along the signal path) as well as the spectral index of a power law irregularity spectrum. However, as shown in Figure 2, for a given irregularity spectrum, d_l becomes nearly independent of H under saturated scintillation conditions ($S_4 \geq 1$). For this figure, the standard deviation (σ_ϕ) of phase variations imposed on the incident radio wave by the irregularity layer as a whole, which in this case would be the fluctuations in vertical TEC, is considered to be 16 radians. Thickness of the

irregularity layer and outer scale for the power law spectrum are taken as 50 km and 10 km, respectively. As the recorded scintillations are produced mainly by irregularities near the F peak, restricting the thickness of the irregularity layer to 50 km is justified. Also, as long as the outer scale is much greater than the Fresnel scale, characteristics of scintillations are not expected to change if the outer scale is altered. A strong dependence of d_i on the irregularity spectral index m is evident in Figure 2. A shallower spectrum indicating the presence of shorter scale length irregularities gives rise to shorter d_i .

For studying the evolution of the irregularity spectrum, the coherence time of saturated scintillations is not useful as the drift velocity of the irregularities across the signal path varies throughout the course of a scintillation event. Also, theoretical results for d_i can be used to interpret d_i derived from scintillation data. For obtaining d_i from spaced receiver amplitude scintillation data, a method was developed by *Bhattacharyya et al.* [2003] which was based on an assumed form of the space-time correlation function for the intensity variations in the moving ground scintillation pattern. This form was first suggested by *Briggs* [1984] for computation of the average drift speed V_0 of the pattern along the baseline of the receivers as well as the random velocity V_C , which accounts for the de-correlation of spaced receiver signals:

$$C_I(x, t) = f \left[(x - V_0 t)^2 + V_C^2 t^2 \right] \quad (1)$$

The x axis here is along the baseline of the receivers, separated by a distance x_0 in the magnetic east-west direction. For the computation of V_0 and V_C , it is only necessary to assume that f is a monotonically decreasing function of its argument with $f(0) = 1$. However, the exact functional form of f is required to characterize the spatial correlation function $C_I(x, 0) = f(x^2)$. According to equation (1), the cross-correlation function of the spaced receiver signals attains its maximum value at a time lag t_m :

$$C_I(x_0, t_m) = f \left[x_0^2 V_C^2 / (V_C^2 + V_0^2) \right] \quad (2)$$

The values of $C_I(x_0, t_m)$, V_C , and V_0 are obtained in the course of a full correlation analysis of spaced receiver scintillation data for a chosen interval of time. It is seen from equation (2) that $C_I(x_0, t_m)$ yields the value of $C_I(x, 0)$ for $x = x_0 V_C / (V_C^2 + V_0^2)^{1/2}$ for the time interval under consideration. Analysis of spaced receiver scintillation data from Ascension Island and Ancon has shown that it is a fairly good approximation to assume a Gaussian form for the spatial correlation function estimated in this manner [*Bhattacharyya et al.*, 2003]. Thus, d_i may be obtained from the values of $C_I(x_0, t_m)$, V_C , and V_0 computed for each time interval using the following:

$$C_I(x_0, t_m) = \exp \left\{ -0.693 x_0^2 V_C^2 / [(V_C^2 + V_0^2) d_i^2] \right\} \quad (3)$$

The above parameters have been computed for every 3 min interval during a scintillation event, except for the intervals when S_4 falls below 0.15 and noise tends to dominate, and also when $C_I(x_0, t_m)$ falls below 0.5 and the approximations made in the full correlation analysis may not be valid. The de-correlation implied by a non-vanishing V_C actually presents an opportunity to identify the dominant scale size for spatial variations in the ground scintillation pattern at different times. If V_C was zero, the maximum cross correlation, $C_I(x_0, t_m)$, between the two signals would always be unity, and it would not be possible to use equation (3) to determine d_i . For weak scintillations ($S_4 \leq 0.5$), any variation in the height of the irregularity layer or the irregularity spectrum would change d_i , while for saturated scintillations ($S_4 \geq 1$), variations in the irregularity strength or the irregularity spectrum would alter d_i . In the intermediate range of S_4 , all three factors contribute to changes in d_i . Variations in d_i as a scintillation event unfolds thus reflect changes in various characteristics of the irregularities as they evolve. The patterns of these changes in d_i derived from spaced receiver scintillation data recorded at Tirunelveli for magnetically quiet days of three different months are shown in Figure 3. For each month, the top panel of the figure is a scatter plot of the points $(x, C_I(x, 0))$ obtained for scintillation events that occurred on different days of that month. The bottom panel shows how the corresponding d_i varied with local time. A greater spread in d_i values is seen in the months of April 2003 and October 2004 than in May 2003. In April 2003 and October 2004, the shortest d_i s are found between 22 LT and a little after midnight. In May 2003, although fewer scintillation events occur, strong scintillations and shortest d_i s are sometimes found several hours after midnight. For this month, there is not as much variation of d_i with the evolution of the irregularities.

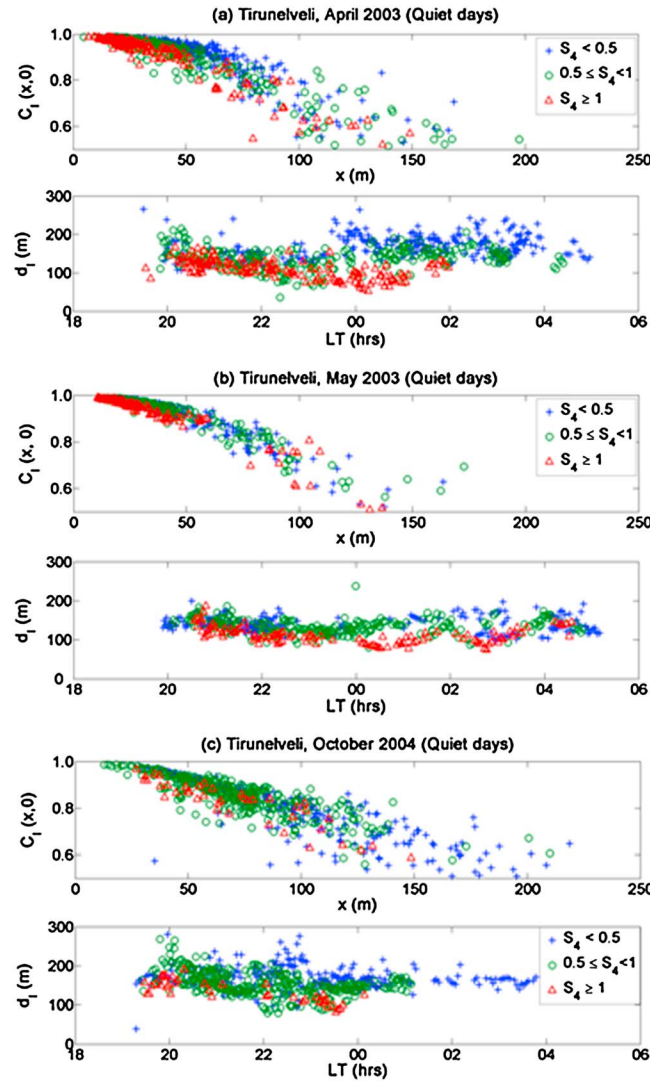


Figure 3. (a) Top panel: scatter plot of the points $(x, C_1(x, 0))$ obtained for scintillation events at the equatorial station Tirunelveli on quiet days in April 2003; bottom panel: local time variation of the corresponding d_1 for April 2003; Figure 3b same as Figure 3a for May 2003; Figure 3c same as Figure 3a for October 2004.

ionosphere, with the reversal of the ambient electric field from eastward to westward, the background ionosphere starts to descend, and according to the simulations by *Krall et al.* [2010] the EPB would quickly stop rising. The EPB would then move down with the background ionosphere to regions where the ion-neutral collision frequency is higher. Therefore, for a given level of density fluctuations, velocity fluctuations associated with the instability are expected to decay fairly rapidly according to equation (4).

Depending on the orientation of the signal path, drift speed V of the ground scintillation pattern along the magnetic east-west baseline of the receivers may have a contribution from the vertical movement of the irregularities as well. With ϕ and θ as the azimuth and zenith angles, respectively, of the signal path, V is given by $V = V_x - V_z \tan \theta \sin \phi$, where V_x and V_z are the eastward and vertical components of the irregularity drift velocity. V is a combination of an average drift V_0 and a fluctuating part. Considering the orientations of the signal paths for UFO2 and FLEETSAT, contributions of V_z to V are $0.13 V_z$ and $0.1 V_z$ respectively, in the two cases. Thus, if V_C is linked with σ_V it is expected to be large only in the initial stage of EPB development, as has been observed in past analysis of spaced receiver scintillation data [*Vacchione et al.*, 1987; *Spatz et al.*, 1988; *Bhattacharyya et al.*, 1989]. Further, it has been suggested that the de-correlation of spaced receiver signals in the initial stage may

4. Relationship Between V_C and d_1

As far as scintillations are concerned, a complex three-dimensional structure of the irregularities is accounted for by the irregularity spectrum in the appropriate plane. No matter what the complexity of the structure, as long as it is unchanged while the irregularities drift across the signal paths with a uniform speed, signals recorded by the two spaced receivers would remain correlated and V_C would be zero. In the case of irregularities that drift across the signal path with an average speed V_0 accompanied by random fluctuations in the drift speed having a standard deviation σ_V , theoretical modeling of the space-time variation of the ground intensity pattern for different scintillation regimes and irregularity characteristics has been carried out in the past [*Wernik et al.*, 1983; *Franke*, 1987; *Bhattacharyya et al.*, 1989]. These studies demonstrate that the random velocity V_C introduced in equation (1) may be interpreted as a measure of σ_V , which itself may be related to the standard deviation of plasma density fluctuations produced by the non-linear growth of the R-T instability [*Bhattacharyya et al.*, 1989]:

$$\sigma_V^2 = 0.5 \left(\frac{g}{v_i} \right)^2 \left\langle \frac{|\delta n|^2}{n_0^2} \right\rangle \quad (4)$$

Here v_i is the ion-neutral collision frequency, δn is the variation in plasma density, and n_0 is the background plasma density. In the post-sunset equatorial

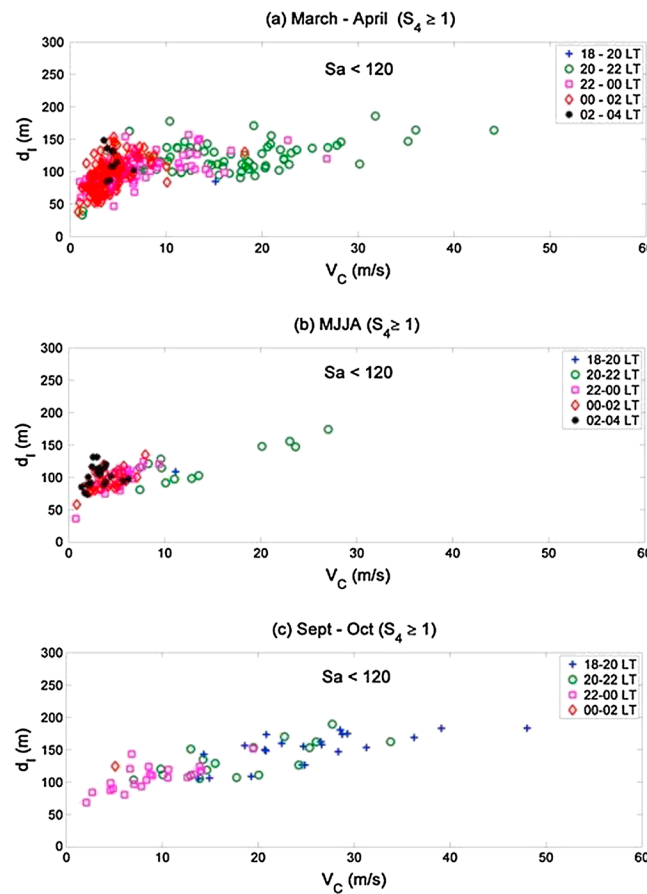


Figure 4. Scatter plot of d_i versus V_C obtained for all 3 min intervals with $S_4 \geq 1$ on quiet days with $S_a < 120$ during (a) March and April; (b) May, June, July, and August (MJJA); and (c) September and October.

be considered as the signature of a nascent EPB [Bhattacharyya *et al.*, 2001; Kakad *et al.*, 2007]. On the other hand, it may also be argued that changes in spatial structure of the irregularities give rise to a non-vanishing V_C . However, it should be noted that changes in spatial structure at scale sizes that would cause the observed de-correlation of scintillations recorded by spaced receivers would alter the intermediate-scale irregularity spectrum and hence d_i .

In order to narrow down the irregularity characteristics that contribute to variations in d_i , the relationship between V_C and d_i is examined only for saturated scintillation conditions ($S_4 \geq 1$). In Figure 4, results obtained from scintillation events that occurred on days with low solar flux conditions ($S_a < 120$) during different seasons are shown. Figure 4a is a scatter plot of d_i versus V_C for 3 min intervals with $S_4 \geq 1$, on magnetically quiet days during the equinoctial months of March and April. Figure 4b is for the summer solstice months of May, June, July, and August (MJJA), while Figure 4c is for equinoctial months of September and October. For low solar flux conditions, there are very few scintillation events with $S_4 \geq 1$ during the months of November, December, January, and

February (NDJF). Asymmetry between vernal and autumnal equinoxes [Ren *et al.*, 2011; Sripathi *et al.*, 2011] is also seen in Figure 4, with greater occurrence of strong scintillations during the vernal compared to the autumnal equinox. On quiet days, the largest values of V_C are generally seen before 22 LT, which pertains to the initial phase of EPB development. The values of V_C during this initial phase are larger during the equinoctial months compared to those obtained for the summer solstice. As discussed earlier, for saturated scintillations d_i is expected to be independent of the height of the irregularity layer and depends only on the spectrum and strength of the irregularities. In Figure 4, the spread in d_i for the summer months is seen to be much less than that found during the equinoxes, although saturated scintillations are seen for a longer duration in the post-midnight period than in the equinoxes, particularly the autumnal equinox, when such scintillations were nearly absent after midnight. This indicates that for the summer solstice, the non-linear evolution of the R-T instability ultimately yields irregularities which do not decay for a long time, so that the strength and the spectrum of the irregularities remain unaltered several hours after midnight. This is seen in Figure 3 as well. Results obtained from scintillation events that occurred on days with moderate to high solar flux conditions ($S_a > 170$) during different seasons are displayed in Figure 5. A scatter plot of d_i versus V_C for saturated scintillations ($S_4 \geq 1$) on magnetically quiet days during the equinoctial months of March and April is shown in Figure 5a, for the summer solstice months (MJJA) in Figure 5b, for equinoctial months of September and October in Figure 5c, and for the winter solstice months (NDJF) in Figure 5d. As expected, there are many more events with saturated scintillations for the higher solar flux days compared to the low solar flux conditions considered in Figure 4. Comparisons of Figures 4a and 5a, Figures 4b and 5b, and Figures 4c and 5c bring out the fact that larger values of V_C are obtained on high solar flux days as compared to low solar flux days. Also, irrespective of

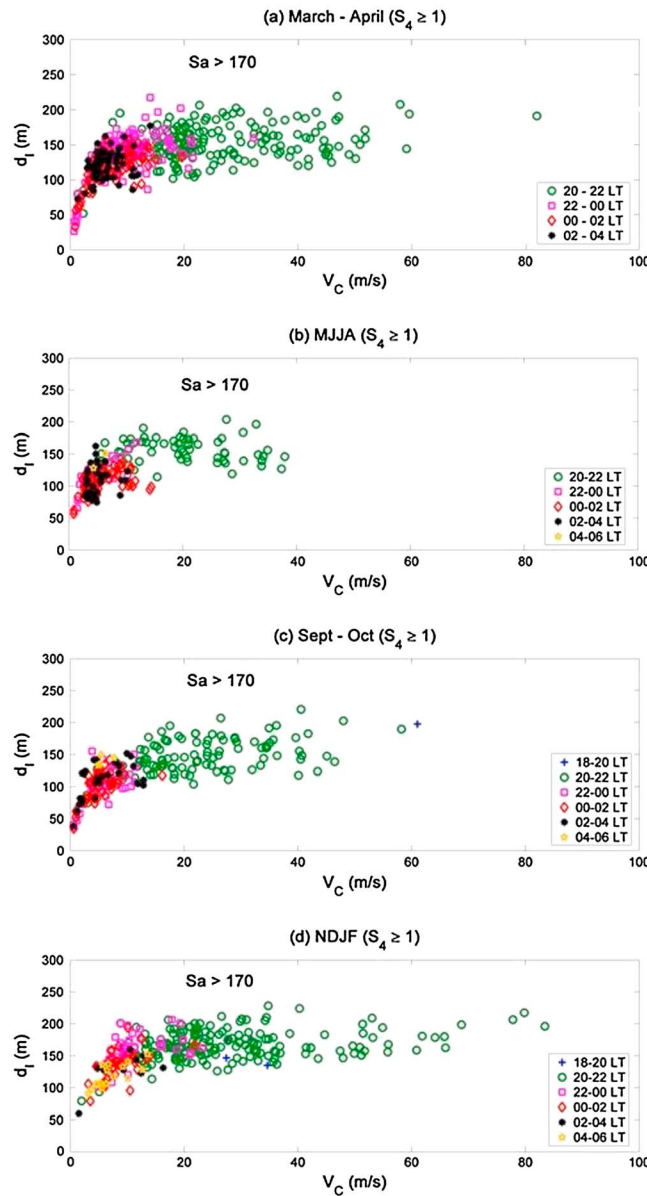


Figure 5. Scatter plot of d_l versus V_C obtained for all 3 min intervals with $S_4 \geq 1$ on quiet days with $S_a > 170$ during (a) March and April; (b) May, June, July, and August (MJA); (c) September and October; and (d) November, December, January, and February (NDJF).

saturated scintillations, show that during the initial phase of irregularity development, when V_C assumes large values, d_l does not show any large systematic changes, indicating that the spatial structure of the intermediate-scale length irregularities near the F layer peak does not undergo much change, although the height of the F layer peak may be variable. This suggests that V_C may be linked with fluctuations in the drift velocity of the irregularities rather than structural changes in the intermediate-scale irregularities. This hypothesis is strongly supported by the fact that growth of the R-T instability implies the presence of fluctuating electric fields associated with the density perturbations, and these would give rise to variations in the irregularity velocity within an EPB as modeled by *Huba and Joyce* [2010] and observed by C/NOFS (Communication and Navigation Outage Forecasting System) measurements [*Huang et al.*, 2010]. Global models of quiet time vertical drifts of the ambient equatorial ionospheric plasma, developed by *Fejer et al.* [2008] using data from ROCSAT-1 satellite observations, describe the seasonal and solar flux

season, V_C is largest before 22 LT, falling to values ≤ 20 m/s thereafter, while d_l does not vary significantly until V_C falls below 20 m/s. The shortest coherence scales d_l appear only after V_C falls to small values below 10 m/s. The possible implications of these results for the evolution of intermediate-scale length irregularities in the post-sunset equatorial ionosphere through the non-linear development of the R-T instability are discussed in the next section.

5. Discussion and Summary

Scintillations recorded by the receivers are an integrated effect of all the irregularities along the signal path, with maximum contribution coming from the region around the F layer peak. In Figure 3, all levels of scintillations are included. It is known from observations [*Bhattacharyya et al.*, 2003, and other references therein] that d_l is largest for weak scintillations and decreases with increasing irregularity strength, for which the S_4 index is not a good proxy when the scintillations are saturated. In Figure 3, large variations in d_l for weak scintillations ($S_4 < 0.5$) are mostly due to the day-to-day variability in the height of the F layer peak. For moderate to strong scintillations ($0.5 \leq S_4 < 1$), the height of the F layer peak plays a less important role, and irregularity strength and spectrum also contribute to the variations. For saturated scintillations ($S_4 \geq 1$), d_l is independent of the height of the F layer peak and only depends on irregularity strength and spectrum. Figures 4 and 5, which consider only

dependence of the drifts in different longitude zones. According to these models, for solar flux index $S_a = 130$ as well as for $S_a = 200$, the evening pre-reversal enhancements of the upward drift in the Indian region are much smaller for the summer solstice months extending from May to August compared to those for the equinoxes. Thus, the maximum height reached by the equatorial ionosphere during post-sunset hours would be much greater during the equinoxes compared to the summer solstice. According to equation (4), the greater the height of the post-sunset equatorial ionosphere, the smaller would be the ion-neutral collision frequency, yielding higher values of σ_v in the initial phase of irregularity development. This would explain why V_c attains higher values in equinox compared to the summer solstice, for the same solar flux conditions. The models developed by *Fejer et al.* [2008] also show that for the same season, the evening pre-reversal enhancements of the upward drift are significantly greater for $S_a = 200$ than for $S_a = 130$. This too supports the results displayed in Figures 4 and 5, which are for $S_a < 120$ and $S_a > 170$, respectively.

For moderate to high solar flux conditions ($S_a > 170$), there are events with saturated VHF scintillations ($S_4 \geq 1$) extending beyond 02 LT in all the seasons. However, under low solar flux conditions ($S_a < 120$), there is greater occurrence of saturated scintillations beyond 02 LT during summer solstice than during equinoxes, with such scintillations rarely extending beyond midnight during September and October. This is seen to be the case for VHF scintillations recorded in Nairobi, Kenya, during magnetically quiet times in the low solar flux years of 2010–2012 [*Yizengaw et al.*, 2013]. Although there are very few events with saturated scintillations during the NDJF months for low solar flux conditions, for $S_a > 170$ largest number of intervals beyond 04 LT with saturated scintillations were found in the NDJF months. This may be attributed to the late sunrise during these months. From Figures 4 and 5, it is concluded that during the non-linear development of the R-T instability in a dynamic background, the electric field fluctuations that give rise to V_c grow and decay without any major change in the intermediate-scale plasma density structures near the equatorial F region peak. Spectrum of intermediate-scale irregularities in the F peak region tends to be shallower after the EPBs are fossilized, yielding the shortest values of d_f after 22 LT, particularly during the summer solstice.

This does not preclude the possibility that in the pre-midnight period the irregularity spectrum would be fully developed on the topside of the equatorial F region. On the basis of a spectral analysis of plasma drift data from AE-E satellite during its passage through strong spread F irregularities, which would map along geomagnetic field lines to apex heights of ~ 600 – 900 km in the topside equatorial F region, *Shume and Hysell* [2004] found a one-dimensional spectral slope close to $-5/3$, indicative of an inertial regime, for irregularities in the scale length range of about 1 to 100 km. Their results could not be extended below 1 km on account of the instrument noise floor. Spectral analysis of high-resolution ion density data from the low-inclination C/NOFS satellite has yielded a spectral slope close to $-5/3$ in the intermediate-scale range [*Rodrigues et al.*, 2009]. As these measurements are from an altitude of ~ 450 km, the authors explained their observation of an inertial regime at this altitude to be due to the extended solar minimum conditions, which saw unusually low neutral densities and consequently much lower ion-neutral collision frequencies at this altitude. On the basis of results presented here, which are obtained from VHF scintillation observations and therefore pertain to intermediate-scale irregularities in the region near the equatorial F layer peak, and the spectra of irregularities in the topside equatorial F region obtained by *Shume and Hysell* [2004] and *Rodrigues et al.* [2009], it is suggested that in the early phase of development of the EPBs, before about 22 LT, the EPBs may be more structured in the topside equatorial F region than near the F layer peak. This picture of the development of structure within the EPBs is supported by fluxgate magnetometer data collected during the years 2000–2005 by the Challenging Mini-satellite Payload (CHAMP), which have been used to investigate irregularity structure in EPBs [*Xiong et al.*, 2012]. These authors have analyzed the variations of the magnetic field component parallel to the main geomagnetic field, which correlate well with electron density variations on account of the diamagnetic effect. They considered several different ranges of scale sizes by applying appropriate filters to the data and found that shorter scale structures are found preferably on flux tubes with increasingly larger L-values (their Figure 7). Occurrence of the shortest scales considered by them in the range of 15–76 km was found to maximize on flux tubes with an apex height of about 800 km at all longitudes. They also found the occurrence rate of these structures to decrease after 22 LT.

Intermediate-scale irregularities in the topside equatorial F region would map down, along geomagnetic field lines, to a region near the crest of the equatorial anomaly, where the higher ambient ionization density would result in stronger irregularities than those in the topside equatorial F region. Strong L-band scintillations are

therefore more likely to appear near the anomaly crest as has been observed. Near the dip equator, the topside equatorial irregularities would give rise to weak scintillations on a VHF signal and even weaker scintillations on an L-band signal. However, irregularities near the F region peak with a steeper spectrum, implying the absence of irregularities of a few 100 m scale size, would contribute more to VHF scintillations. Thus, in the equatorial region, strong VHF scintillations would not be accompanied by strong L-band scintillations, which would be seen only in the anomaly crest region in the pre-midnight hours. This pattern of VHF and L-band scintillation occurrence has been extensively reported in the past [Mullen *et al.*, 1985; Groves *et al.*, 1997; Bhattacharyya *et al.*, 2003; Sripathi *et al.*, 2008] as stated in the introduction. In the past, this has been attributed only to the higher ambient plasma density near the EIA crest. On the basis of the present study, a scenario is suggested where greater structuring of the EPB near the F region peak may be seen away from the dip equator than in equatorial region in the early stages of intermediate-scale irregularity development within an EPB, and this would also contribute to stronger L-band scintillations observed near the crest of the EIA. In the post-midnight hours, after the perturbation electric fields associated with the R-T instability decay, the irregularities also descend with the ambient plasma, and with the equatorial F region at a lower height, the top side irregularities would no longer map to the EIA crest region, and the L-band scintillations there would cease. Development of a shallow irregularity spectrum near the peak of the equatorial F region at this time may produce strong scintillations on a VHF signal but not on an L-band signal since the background plasma density is much reduced compared to the pre-midnight period, and the shortest d_f obtained at the dip equator would still be much larger than the shortest d_f obtained near the anomaly crest as was found to be the case for Ancon and Ascension Island [Bhattacharyya *et al.*, 2003]. In the future, three-dimensional simulations of the development of an EPB with better spatial resolution may be able to demonstrate the evolution of the intermediate-scale length irregularities at different heights within an EPB.

Acknowledgments

A. Bhattacharyya acknowledges the support received from SERB, Department of Science and Technology, Government of India, in the form of a J. C. Bose National Fellowship.

Robert Lysak thanks Chao Xiong and an anonymous reviewer for their assistance in evaluating this paper.

References

- Basu, S., S. Basu, J. P. McClure, W. B. Hanson, and H. E. Whitney (1983), High resolution topside data of electron densities and VHF/GHz scintillations in the equatorial region, *J. Geophys. Res.*, *88*, 403–415.
- Bhattacharyya, A., and K. C. Yeh (1988), Intensity correlation function for waves of different frequencies propagating through a random medium, *Radio Sci.*, *23*, 791–808.
- Bhattacharyya, A., S. J. Franke, and K. C. Yeh (1989), Characteristic velocity of equatorial F region irregularities determined from spaced receiver scintillation data, *J. Geophys. Res.*, *94*, 11,959–11,969.
- Bhattacharyya, A., S. Basu, K. M. Groves, C. E. Valladares, and R. Sheehan (2001), Dynamics of equatorial F region irregularities from spaced receiver scintillation observations, *Geophys. Res. Lett.*, *28*, 119–122.
- Bhattacharyya, A., K. M. Groves, S. Basu, H. Kuenzler, C. E. Valladares, and R. Sheehan (2003), L-band scintillation activity and space-time structure of low-latitude UHF scintillations, *Radio Sci.*, *38*(1), 1004, doi:10.1029/2002RS002711.
- Briggs, B. H. (1984), The analysis of spaced sensor records by correlation techniques, in *Middle Atmosphere Program, Handbook for MAP*, vol. 13, edited by R. A. Vincent, pp. 166–186, ICSU, Paris.
- Costa, E., E. R. de Paula, L. F. C. Rezende, K. M. Groves, P. A. Roddy, E. V. Dao, and M. C. Kelley (2011), Equatorial scintillation calculations based on coherent scatter radar and C/NOFS data, *Radio Sci.*, *46*, RS2011, doi:10.1029/2010RS004435.
- Engavale, B., and A. Bhattacharyya (2005), Spatial correlation function of intensity variations in the ground scintillation pattern produced by equatorial spread F irregularities, *Indian J. Radio Space Phys.*, *34*, 23–32.
- Fejer, B. G., J. W. Jensen, and S.-Y. Su (2008), Quiet time equatorial F region vertical plasma drift model derived from ROCSAT-1 observations, *J. Geophys. Res.*, *113*, A05304, doi:10.1029/2007JA012801.
- Franke, S. (1987), The space-time intensity correlation function of scintillation due to a deep random phase screen, *Radio Sci.*, *22*, 4, doi:10.1029/RS022i004p00643.
- Franke, S. J., and C. H. Liu (1985), Modeling of equatorial multifrequency scintillation, *Radio Sci.*, *20*, 403–415.
- Groves, K. M., et al. (1997), Equatorial scintillation and systems support, *Radio Sci.*, *32*, 2047–2064.
- Huang, C.-S., O. de La Beaujardiere, R. F. Pfaff, J. M. Retterer, P. A. Roddy, D. E. Hunton, Y.-J. Su, S.-Y. Su, and F. J. Rich (2010), Zonal drift of plasma particles inside equatorial plasma bubbles and its relation to the zonal drift of the bubble structure, *J. Geophys. Res.*, *115*, A07316, doi:10.1029/2010JA015324.
- Huba, J., and G. Joyce (2010), Global modeling of equatorial plasma bubbles, *Geophys. Res. Lett.*, *37*, L17104, doi:10.1029/2010GL044281.
- Kakad, B., K. Jeeva, K. U. Nair, and A. Bhattacharyya (2007), Magnetic activity linked generation of nighttime equatorial spread F irregularities, *J. Geophys. Res.*, *112*, A07311, doi:10.1029/2006JA012021.
- Kakad, B., C. K. Nayak, and A. Bhattacharyya (2012), Power spectral characteristics of ESF irregularities during magnetically quiet and disturbed days, *J. Atmos. Sol. Terr. Phys.*, *81–82*, 41–49.
- Krall, J., J. D. Huba, S. L. Ossakow, and G. Joyce (2010), Why do equatorial ionospheric bubbles stop rising?, *Geophys. Res. Lett.*, *37*, L09105, doi:10.1029/2010GL043128.
- Mullen, J. P., E. Mackenzie, S. Basu, and H. Whitney (1985), UHF/GHz scintillation observed at Ascension Island from 1980 through 1982, *Radio Sci.*, *20*, 357–365.
- Ren, Z., W. Wan, L. Liu, Y. Chen, and H. Le (2011), Equinoctial asymmetry of ionospheric vertical plasma drifts and its effect on F-region plasma density, *J. Geophys. Res.*, *116*, A02308, doi:10.1029/2010JA016081.
- Retterer, J. M. (2010a), Forecasting low-latitude radio scintillation with 3-D ionospheric plume models: 1. Plume model, *J. Geophys. Res.*, *115*, A03306, doi:10.1029/2008JA013839.

- Retterer, J. M. (2010b), Forecasting low-latitude radio scintillation with 3-D ionospheric plume models: 2. Scintillation calculation, *J. Geophys. Res.*, *115*, A03307, doi:10.1029/2008JA013840.
- Rino, C. L., and J. Owen (1980), The time structure of transionospheric radio wave scintillation, *Radio Sci.*, *15*, 479–489.
- Rodrigues, F. S., M. C. Kelley, P. A. Roddy, D. E. Hunton, R. F. Pfaff, O. de La Beaujardière, and G. S. Bust (2009), C/NOFS observations of intermediate and transitional scale-size equatorial spread F irregularities, *Geophys. Res. Lett.*, *36*, L00C05, doi:10.1029/2009GL038905.
- Shume, E. B., and D. L. Hysell (2004), Spectral analysis of plasma drift measurements from the AE-E satellite: Evidence of an inertial subrange in equatorial spread F, *J. Atmos. Sol. Terr. Phys.*, *66*, 57–65.
- Spatz, D. E., S. J. Franke, and K. C. Yeh (1988), Analysis and interpretation of spaced receiver scintillation data recorded at an equatorial station, *Radio Sci.*, *23*, 347–361.
- Sripathi, S., S. Bose, A. K. Patra, T. K. Pant, B. Kakad, and A. Bhattacharyya (2008), Simultaneous observations of ESF irregularities over Indian region using radar and GPS, *Ann. Geophys.*, *26*, 3197–3213.
- Sripathi, S., B. Kakad, and A. Bhattacharyya (2011), Study of equinoctial asymmetry in the Equatorial Spread F (ESF) irregularities over Indian region using multi-instrument observations in the descending phase of solar cycle 23, *J. Geophys. Res.*, *116*, A11302, doi:10.1029/2011JA016625.
- Vacchione, J. D., S. J. Franke, and K. C. Yeh (1987), A new analysis technique for estimating zonal irregularity drifts and variability in the equatorial F region using spaced receiver scintillation data, *Radio Sci.*, *22*, 745–756.
- Valladares, C. E., J. Villalobos, R. Sheehan, and M. P. Hagan (2004), Latitudinal extension of low-latitude scintillations measured with a network of GPS receivers, *Ann. Geophys.*, *22*, 3155.
- Wernik, A., C. Liu, and K. Yeh (1983), Modeling of spaced-receiver scintillation measurements, *Radio Sci.*, *18*, 743–764, doi:10.1029/RS018i005p00743.
- Xiong, C., H. Lüher, S. Y. Ma, C. Stolle, and B. G. Fejer (2012), Features of highly structured equatorial plasma irregularities deduced from CHAMP observations, *Ann. Geophys.*, *30*, 1259–1269.
- Yeh, K. C., and C. H. Liu (1982), Radio wave scintillations in the ionosphere, *Proc. IEEE*, *70*(4), 324–358.
- Yizengaw, E., J. Retterer, E. E. Pacheco, P. Roddy, K. Groves, R. Caton, and P. Baki (2013), Post-midnight bubbles and scintillations in the quiet-time June solstice, *Geophys. Res. Lett.*, *40*, 5592–5597, doi:10.1002/2013GL058307.